Обзор arXiv: astro-ph, February 20-24, 2017

От Сильченко О.К.

Astro-ph: 1702.05485

KINETyS: Constraining spatial variations of the stellar initial mass function in early-type galaxies ⋆

Padraig D. Alton[1]†, Russell J. Smith[1], and John R. Lucey[1]
[1] *Centre for Extragalactic Astronomy, Department of Physics, Durham University, South Road, Durham DH1 3LE, UK*

Submitted 21 February 2017

ABSTRACT

The heavyweight stellar initial mass function (IMF) observed in the cores of massive early-type galaxies (ETGs) has been linked to formation of their cores in an initial swiftly-quenched rapid starburst. However, the outskirts of ETGs are thought to be assembled via the slow accumulation of smaller systems in which the star formation is less extreme; this suggests the form of the IMF should exhibit a radial trend in ETGs. Here we report radial stellar population gradients out to the half-light radii of a sample of eight nearby ETGs. Spatially resolved spectroscopy at 0.8–1.35μm from the VLT's KMOS instrument was used to measure radial trends in the strengths of a variety of IMF-sensitive absorption features (including some which are previously unexplored). We find weak or no radial variation in some of these which, given a radial IMF trend, ought to vary measurably, e.g. for the Wing-Ford band we measure a gradient of $+0.06 \pm 0.04$ per decade in radius.

Выборка

Table 1. List of sample galaxies with observation details and key properties listed. Effective radii and total (J-band) magnitudes within the effective radius were extracted from 2MASS J-band images and used to calculate the mean surface brightness. Recession velocities were derived using pPXF (see Section 2.3) and $\sigma(\mathrm{R_{eff}}/8)$ values and fast/slow rotator status were taken from the ATLAS 3D survey (except for NGC 1407 for which a value was derived from our pPXF fits). Relative M/L taken from CvD12b.

Name	Bands	Seeing /arcsec	$\mathrm{R_{eff}}$ /arcsec	cz $/\mathrm{kms}^{-1}$	$\sigma(\mathrm{R_{eff}}/8)$ $/\mathrm{kms}^{-1}$	surface brightness $/\mathrm{mag}_J\ \mathrm{arcsec}^{-2}$	relative M/L (Milky Way = 1)	ellipticity	Notes
NGC 0524	IZ,YJ	1.3, —	23.3	2400	243	17.8	1.09	0.00	Fast rotator
NGC 1407	IZ	1.4, 1.0	36.2	1950	301	17.4	—	0.00	Slow rotator
NGC 3377	IZ,YJ	1.8, —	23.3	690	146	17.0	1.16	0.40	Fast rotator
NGC 3379	IZ	1.2, 0.8	28.5	900	213	16.5	1.60	0.00	Fast rotator
NGC 4486	IZ,YJ	1.1, 1.3	44.5	1290	314	16.9	1.90	0.00	Slow rotator
NGC 4552	IZ,YJ	1.1, 1.6	24.1	390	262	16.6	2.04	0.00	Slow rotator
NGC 4621	IZ,YJ	1.3, 1.6	27.7	480	224	16.8	1.96	0.33	Fast rotator
NGC 5813	IZ,YJ	1.3, 1.2	33.7	1920	226	17.9	1.37	0.25	Slow rotator

Как стояли поля IFU KMOS

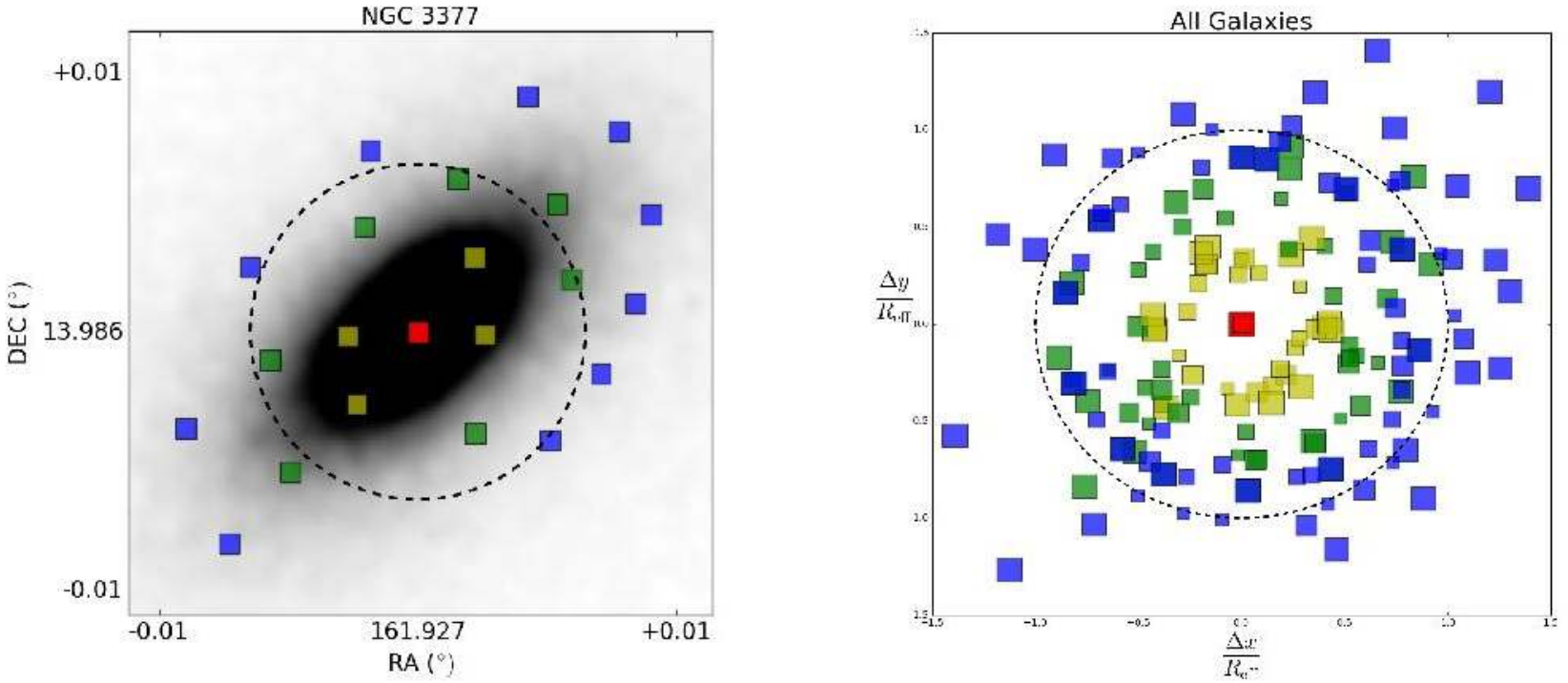

Figure 1. *Left panel:* The KINETyS observing strategy for an example galaxy. Individual KMOS IFU fields of view (2.8″ x 2.8″) are shown to scale, colour coded by the isophote they are sampling. Dashed line indicates the J-band effective radius. *Right Panel:* IFU fields for the ensemble of all galaxies scaled relative to the J-band circular effective radius. Colour scheme as in left panel.

Модельный спектр с интересными линиями

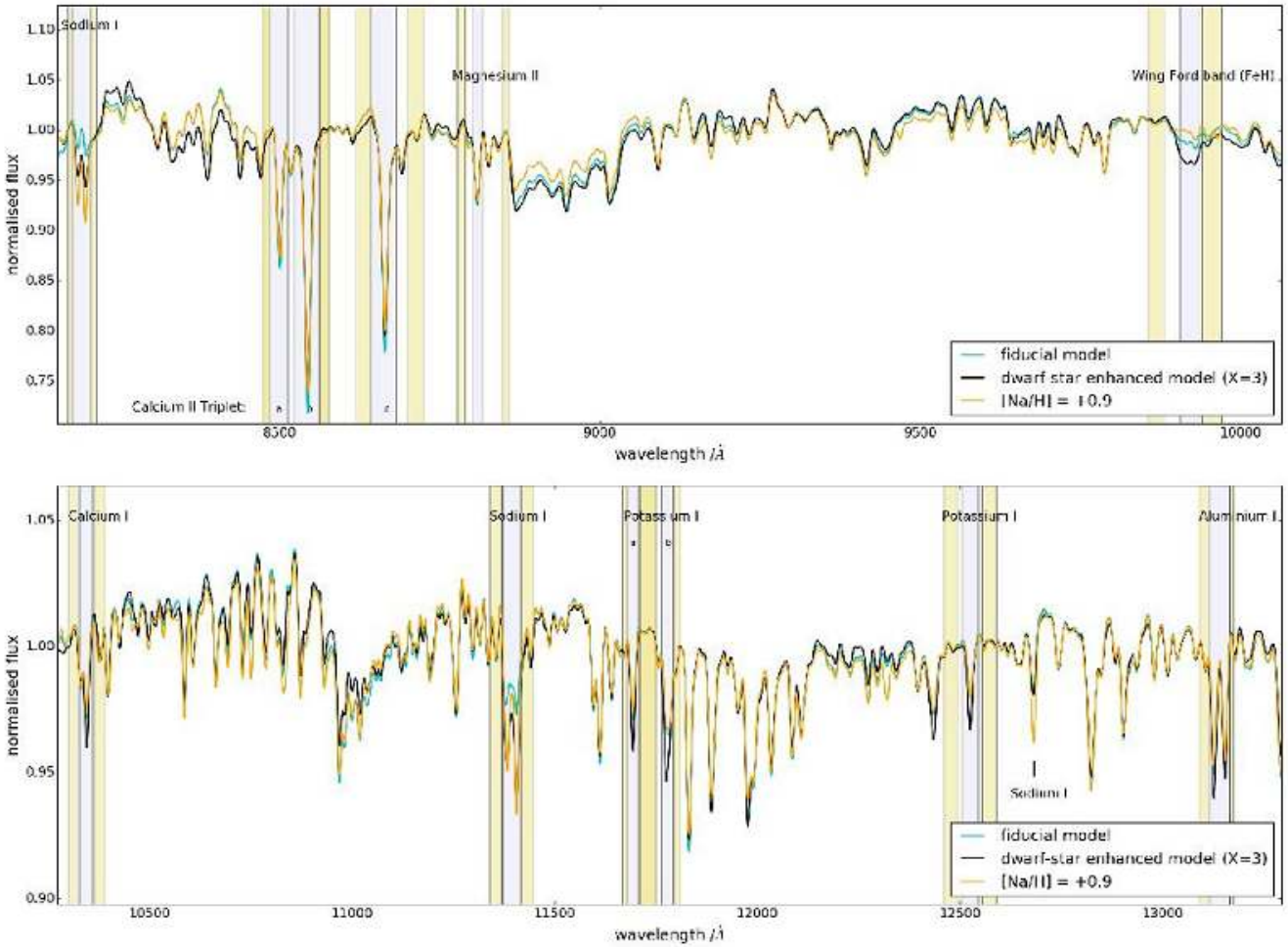

Figure 2. Three models of NIR spectra are illustrated: the solar abundance, Milky-Way-like IMF fiducial model (cyan); a model with [Na/H]$= +0.9$ (orange), and a model with a dwarf-enriched stellar population formed according to an $X = 3$ IMF (black). The models are broadened to 230 kms^{-1} We include

Наблюдаемые спектры, сложенные по всем галактикам на разных расстояниях от центра

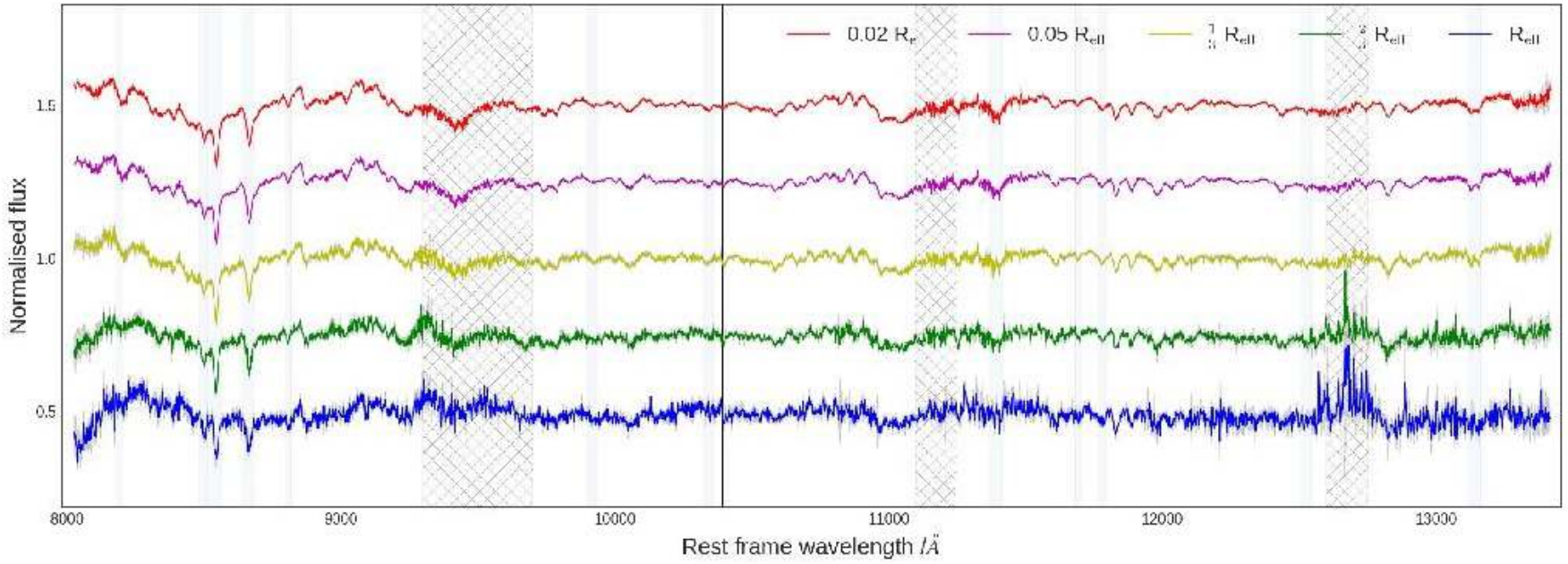

Figure 3. The data, median-stacked at fixed R/R_{eff}, indicating the recovery of the signal in the absorption line spectra even in the outlying regions of the galaxy (feature measurement bands indicated). The colour scheme is as in Fig. 1. The hatched regions indicate particularly strong telluric absorption, visible

Градиенты индексов линий

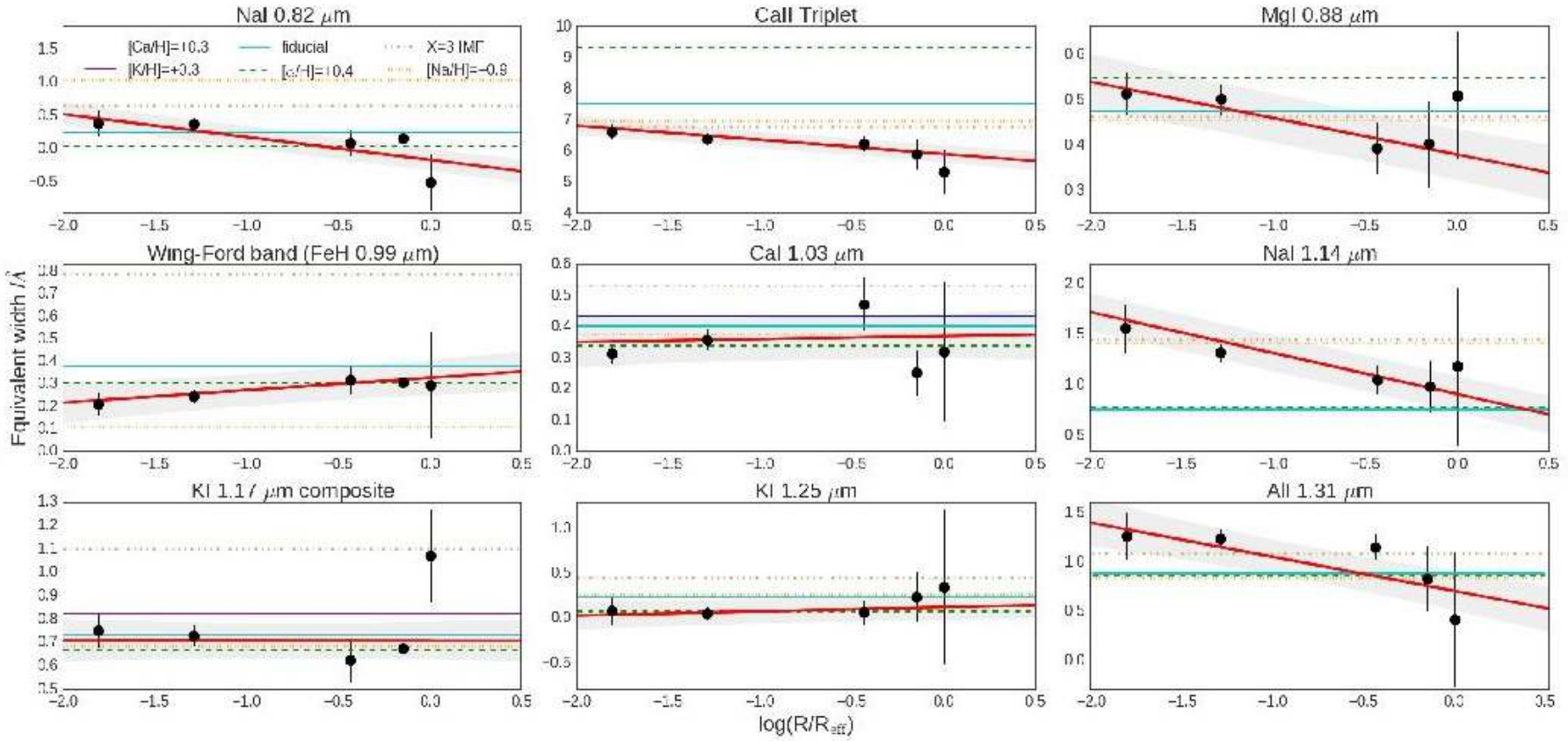

Figure 4. The index trends with $\log(R/R_{\rm eff})$. The index measurements for each radial extraction region (corrected to 230 $\rm kms^{-1}$ in all cases) are shown in black with errors. The best fit trends are in red with the calculated 1σ uncertainty region shown (grey shaded). The SSP model predictions are denoted by horizontal lines (Cyan: fiducial model; Green: [α/H]=+0.4; Tan: X=3 IMF; Orange: [Na/H]=+0.9; Dark blue: [Ca/H]=+0.3 (but note that Ca is also an α-element so scales with [α/H] too); Purple: [K/H]=+0.3)

Градиенты параметров звездного населения: доля карликовых звезд НЕ меняется по радиусу

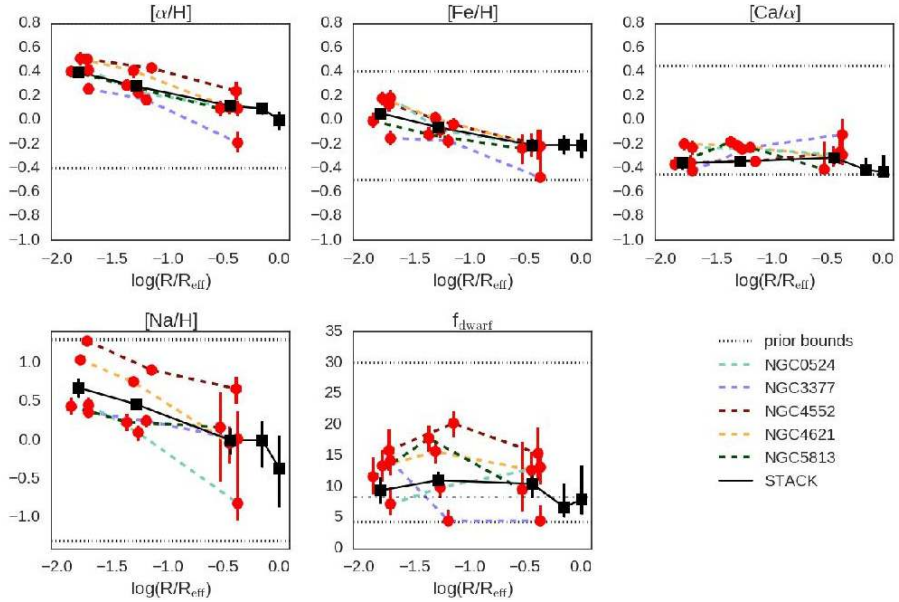

Table 9. Model parameters and best fit values for stacked spectra at five radii

Extraction Region	$[\alpha/H]$	$[Fe/H]$	f_{dwarf}	$[Na/H]$	$[Ca/\alpha]$	reduced χ^2
$R < 0.02\,R_{eff}$	$0.40^{+0.02}_{-0.02}$	$0.06^{+0.03}_{-0.03}$	$9.4^{+2.1}_{-2.1}$	$0.68^{+0.12}_{-0.12}$	$-0.36^{+0.05}_{-0.05}$	0.84
$R = 0.02$–$0.05\,R_{eff}$	$0.28^{+0.02}_{-0.02}$	$-0.06^{+0.03}_{-0.03}$	$11.1^{+1.5}_{-1.5}$	$0.47^{+0.07}_{-0.07}$	$-0.34^{+0.04}_{-0.04}$	2.00
$R = \frac{1}{3}\,R_{eff}$	$0.12^{+0.03}_{-0.03}$	$-0.21^{+0.05}_{-0.05}$	$10.5^{+2.1}_{-2.2}$	$0.00^{+0.15}_{-0.18}$	$-0.31^{+0.06}_{-0.06}$	1.54
$R = \frac{2}{3}\,R_{eff}$	$0.10^{+0.05}_{-0.05}$	$-0.21^{+0.08}_{-0.08}$	$6.7^{+3.9}_{-1.6}$	$0.00^{+0.24}_{-0.35}$	$-0.41^{+0.10}_{-0.02}$	0.35
$R = R_{eff}$	$0.00^{+0.07}_{-0.08}$	$-0.21^{+0.1}_{-0.1}$	$8.0^{+5.6}_{-2.5}$	$-0.36^{+0.43}_{-0.5}$	$-0.43^{+0.14}_{-0.01}$	0.91
best-fit gradients	-0.20 ± 0.01	-0.17 ± 0.02	-0.6 ± 0.8	-0.48 ± 0.07	0.00 ± 0.04	

Astro-ph: 1702.06984

THE AGES OF THE THIN DISK, THICK DISK, AND THE HALO FROM NEARBY WHITE DWARFS

Mukremin Kilic[1], Jeffrey A. Munn[2], Hugh C. Harris[2], Ted von Hippel[3,4], James W. Liebert[5], Kurtis A. Williams[6], Elizabeth Jeffery[7], Steven DeGennaro[8]

Draft version February 24, 2017

ABSTRACT

We present a detailed analysis of the white dwarf luminosity functions derived from the local 40 pc sample and the deep proper motion catalog of Munn et al. (2014, 2017). Many of the previous studies ignored the contribution of thick disk white dwarfs to the Galactic disk luminosity function, which results in an erronous age measurement. We demonstrate that the ratio of thick/thin disk white dwarfs is roughly 20% in the local sample. Simultaneously fitting for both disk components, we derive ages of 6.8-7.0 Gyr for the thin disk and 8.7 $\pm$ 0.1 Gyr for the thick disk from the local 40 pc sample. Similarly, we derive ages of 7.4-8.2 Gyr for the thin disk and 9.5-9.9 Gyr for the thick disk from the deep proper motion catalog, which shows no evidence of a deviation from a constant star formation rate in the past 2.5 Gyr. We constrain the time difference between the onset of star formation in the thin disk and the thick disk to be $1.6^{+0.3}_{-0.4}$ Gyr. The faint end of the luminosity function for the halo white dwarfs is less constrained, resulting in an age estimate of $12.5^{+1.4}_{-3.4}$ Gyr for the Galactic inner halo. This is the first time ages for all three major components of the Galaxy are obtained from a sample of field white dwarfs that is large enough to contain significant numbers of disk and halo objects. The resultant ages agree reasonably well with the age estimates for the oldest open and globular clusters.

Функция светимости белых карликов хорошо описывается только суммой тонкого и толстого диска

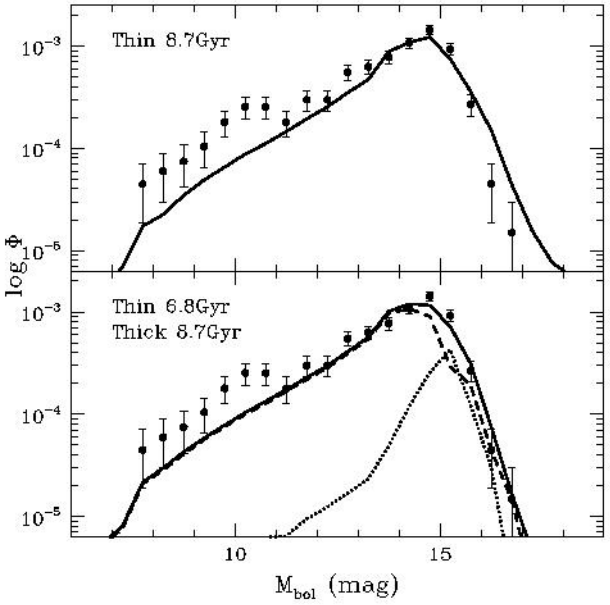

FIG. 2.— The observed luminosity function for the local 40 pc sample of white dwarfs (points with error bars, Limoges et al. 2015) compared to the best-fit synthetic white dwarf luminosity function (solid lines). The top panel shows the model fits assuming a population of 100% thin disk stars, whereas the bottom panel shows the fits using a composite population where the ratio of thick disk to thin disk white dwarfs is 22%. Dashed and dotted lines show the contribution from the thin disk and thick disk white dwarfs,

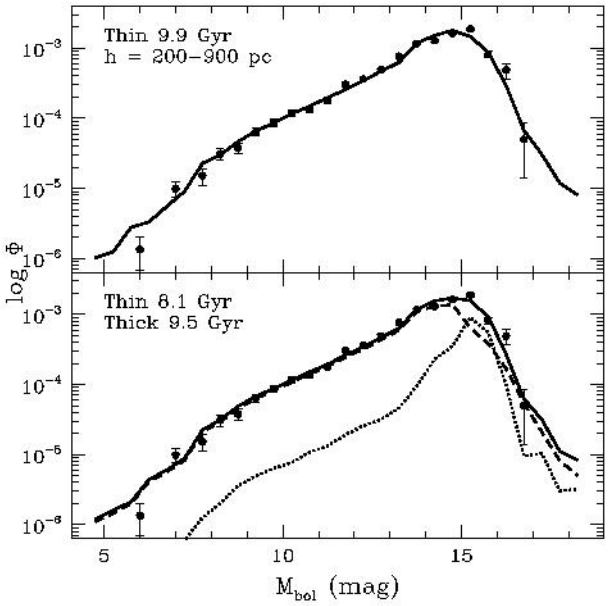

FIG. 6.— The white dwarf luminosity function from the deep proper motion survey (points with error bars, Munn et al. 2017) using a disk scale height range of 200-900 pc. The top panel shows the model fits assuming a population of 100% thin disk stars, whereas the bottom panel shows the fits using a composite population where the ratio of thick disk to thin disk white dwarfs is 35%. Dashed and dotted lines show the contribution from the thin disk and thick

Локальная выборка до 40 пк от Солнца

Глубокий обзор собственных движений Munn et al. (2017)

Другие компоненты Галактики

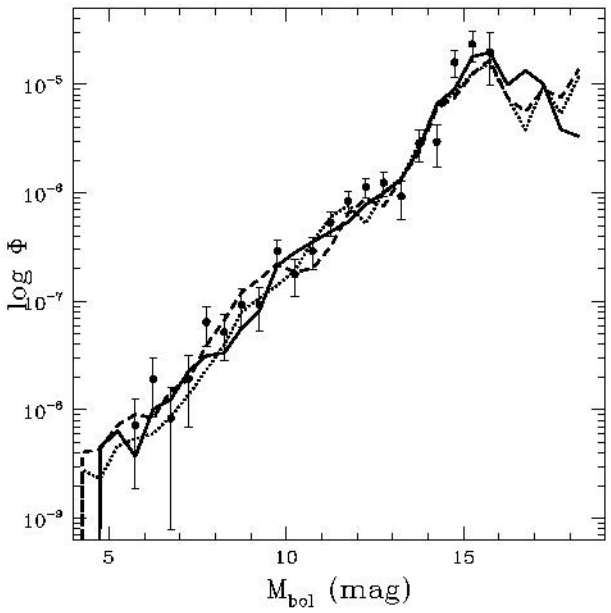

FIG. 9.— Munn et al. (2017) luminosity function for $v_{tan} = 200$-500 km s^{-1} halo white dwarf sample. Solid, dashed, and dotted lines show model luminosity functions for 12.5, 13.9, and 15.0 Gyr old halo samples, respectively. This luminosity function implies a halo age of $12.5^{+1.4}_{-3.4}$ Gyr.

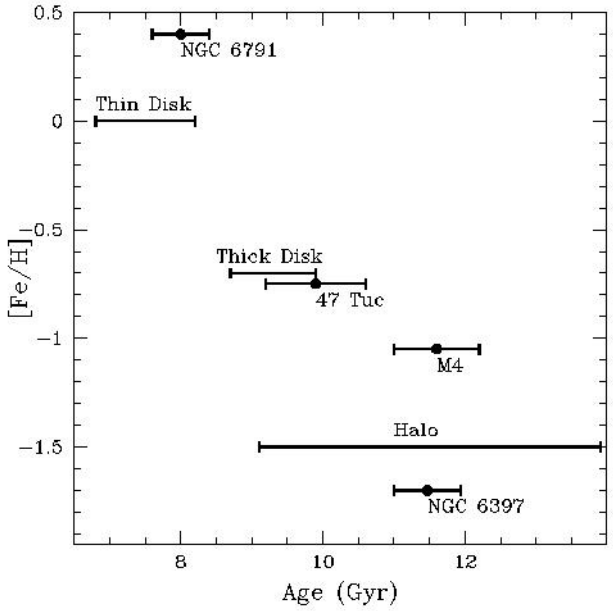

FIG. 10.— Age-Metallicity relation based on the white dwarf luminosity functions for the open cluster NGC 6791, globular clusters 47 Tuc, M4, and NGC 6397 (Hansen et al. 2013, and references therein), and field thin disk, thick disk, and halo stars from this study. The error bars cover the age ranges estimated from both the 40 pc local sample and the Munn et al. (2017) deep proper motion survey sample.

Белые карлики гало

Оценки возрастов по белым карликам для разных компонент

Что интересно:

- Какие выборки не анализируй, как параметры модели не меняй, всегда получается разница эпох начала звездообразования в тонком и толстом диске 1.6+0.3/-0.4 млрд лет – то есть вполне уверенный разрыв во времени.